Origin of Substituent Effects in the Absorption Spectra of Peroxy Radicals: Time Dependent Density Functional Theory Calculations

Jennifer L. Weisman and Martin Head-Gordon*

Contribution from the Department of Chemistry, University of California, Berkeley, and the Chemical Sciences Division, Lawrence Berkeley National Laboratory, Berkeley, California 94720

Received June 4, 2001

Abstract: We investigate the assignment of electronic transitions in alkyl peroxy radicals. Past experimental work has shown that the phenyl peroxy radical exhibits a transition in the visible region; however, previous high level calculations have not reproduced this observed absorption. We use time dependent density functional theory (TDDFT) to characterize the electronic excitations of the phenyl peroxy radical as well as other hydrocarbon substituted peroxy radicals. TDDFT calculations of the phenyl peroxy radical support an excitation in the visible spectrum. Further, we investigate the nature of this visible absorption using electron attachment/detachment density diagrams of the peroxy radicals and present a qualitative picture of the origin of the visible absorption based on molecular orbital perturbations. The peroxy radical substituent is also compared against isoelectronic radical groups. The visible absorption is determined to be dependent on mixing of the alkyl and radical substituent orbitals.

Introduction

Peroxy radicals play an important role in a variety of systems, such as hydrocarbon oxidation reactions and oxidative biochemical systems. They are of interest in such areas as tropospheric and combustion chemistry. On the basis of the parent peroxy radical,[1] alkyl peroxy radicals would generally be expected to absorb in the ultraviolet region (for a review, see ref 2). However, certain radical systems, for example, the vinyl peroxy radical ($C_2H_3O_2$)[3,4] and the phenyl peroxy radical ($C_6H_5O_2$),[3,5−9] have been observed to absorb in the visible region.

The origin of the visible absorption in only certain alkyl peroxy radicals may be related to the presence of the open-shell orbital on the peroxy radical and its interaction with the alkyl moiety. In particular, it is likely that the proximity of the open-shell orbital to an unsaturated alkyl group is what causes the expected ultraviolet absorption to shift into the visible region.[10] The π electrons of the unsaturated alkyl substituent may couple with the half-occupied orbital of the peroxy group and, thus, lower the excitation energies associated with promoting the radical electron.

In the past, both experimental and theoretical studies have been performed on the absorption spectra of several small alkyl peroxy radicals. Among the alkyl peroxy radicals studied are the phenyl peroxy radical,[3,5−11] the two vinyl peroxy radical isomers ($C_2H_3O_2$),[3,4,10] the methyl peroxy radical (CH_3O_2),[1,4,12] and the hydrogen peroxy radical (HO_2).[1,13,14] The phenyl peroxy radical is particularly interesting in that experimental results show a gas-phase absorption in the visible region at 496.4 nm;[5−7] however, high level multiconfiguration self-consistent field (MCSCF) calculations of Krauss and Osman do not predict a visible absorption for this radical.[10]

The MCSCF calculations of the phenyl peroxy radical[10] show an absorption significantly blue-shifted from the gas-phase experimental results. The phenyl peroxy radical also exhibits an aqueous visible absorption.[3,8,9] Krauss and Osman assert that their gas phase MCSCF results would be substantially red-shifted if solvent effects are accounted for, therefore, matching the aqueous absorption. However, they additionally calculate MCSCF gas-phase absorptions for the *cis*- and *trans*-vinyl peroxy radicals, which match the gas-phase experimental absorptions of Fahr et al.[4] quite well. This seems to indicate that the blue-shifted phenyl peroxy radical MCSCF absorption is due to something other than a lack of solvent effects. In fact, it is likely to be the method itself, because their calculated vinyl absorptions show variations of approximately 100 nm depending on the active space. MCSCF descriptions of excited states are, in principle, reliable for radicals. However, it is probable that the larger size of the phenyl peroxy radical did not allow for the use of a sufficiently large active space, relative to the smaller vinyl peroxy radicals.

Radical excitations are more difficult to characterize than closed shell excitations and have thus far been studied less extensively. Configuration interaction (CI) and coupled cluster (CC) based theories are single reference methods routinely used

* Corresponding author. Fax: (510) 643-1255. E-mail: mhg@cchem.berkeley.edu.

(1) Lightfoot, P. D.; Jemi-Alade, A. A. *J. Photochem. Photobiol.* **1991**, *59*, 1.
(2) Wallington, T. J.; Dagaut, P.; Kurylo, M. J. *Chem. Rev.* **1992**, *92*, 667.
(3) Mertens, R.; von Sonntag, C. *Angew. Chem., Int. Ed. Engl.* **1994**, *33*, 1262.
(4) Fahr, A.; Laufer, A. H.; Krauss, M.; Osman, R. *J. Phys. Chem. A* **1997**, *101*, 4879.
(5) Yu, T.; Lin, M. C. *J. Am. Chem. Soc.* **1994**, *116*, 9571.
(6) Yu, T.; Lin, M. C. *J. Phys. Chem.* **1995**, *99*, 8599.
(7) Sommeling, P. M.; Mulder, P.; Louw, R.; Avila, D. V.; Lusztyk, J.; Ingold, K. U. *J. Phys. Chem.* **1993**, *97*, 8361.
(8) Alfassi, A. B.; Khaikin, G. I.; Neta, P. *J. Phys. Chem.* **1995**, *99*, 265.
(9) Fang, X.; Mertens, R.; von Sonntag, C. *J. Chem. Soc., Perkins Trans. 2* **1995**, *6*, 1033.
(10) Krauss, M.; Osman, R. *J. Phys. Chem.* **1995**, *99*, 11387.
(11) Fadden, M. J.; Barckholtz, C.; Hadad, C. M. *J. Phys. Chem. A* **2000**, *104*, 3004.
(12) Herrmann, H.; Reese, A.; Wicktor, F.; Zellner, R. *THEOCHEM* **1997**, *408/409*, 539.
(13) Langhoff, S. R.; Jaffe, R. L. *J. Chem. Phys.* **1979**, *71*, 1475.
(14) Shih, S.-K.; Peyerimhoff, S. D.; Buenker, R. J. *Chem. Phys.* **1978**, *28*, 299.

10.1021/ja011368e CCC: $20.00
Published on Web 10/31/2001

to investigate closed shell excited states; however, relatively few open shell system excited-state studies have been performed.

Maurice and Head-Gordon investigated configuration interaction with single substitutions (CIS) for open shell species, both with unrestricted (UCIS) and restricted open shell (ROCIS) spin orbitals.[15] ROCIS performed slightly better than UCIS; however, both methods predicted excitation energies in error of up to 1−5 eV from experiment. They determined a class of double excitations that play an important role in open shell excitations and, thus, account for a large portion of the inaccuracy seen in the absorption spectra of UCIS and ROCIS. Maurice and Head-Gordon subsequently developed an extended CIS (XCIS) method built upon ROCIS to include this class of important double excitations.[16] XCIS is an improvement over ROCIS, reducing errors by 1−2 eV in very difficult cases; however, it may sometimes predict excited states in error of experiment by a few electronvolts or predict a wrong ordering of states,[16,17] as it does not include dynamical correlation.

Equation of motion and linear response theory coupled cluster methods (EOM-CC and CC-LRT) have been used to calculate excitation energies of a limited number of open shell systems. Comeau and Bartlett demonstrated the ability to use an open shell reference for EOM-CC with single and double substitutions (EOM-CCSD) to accurately calculate excitation energies.[18] Their open shell reference excitation energies agreed with their closed shell reference excitation energies to within less than 0.1 eV for the Be triplet excited states.

EOM-CCSD was later used by Szalay,[19] and subsequently by Szalay et al.,[20] to investigate the excited states of true radicals, the thioketenyl (HCCS) and ketenyl (HCCO) radicals, respectively. Both investigations determined excitation energies in error of experiment by about 3000 cm^{-1}, which is a little over a third of an electronvolt. This accuracy is significantly higher than that of the CIS methods, however, lower than the accuracy expected for closed shell systems.

Szalay and Gauss recently employed spin-restricted CC-LRT as a promising means to calculate radical excitation energies.[21] They found that a class of triple excitations, analogous to the double excitations included in the XCIS work,[16] improved CCSD-LRT excitation energies by as much as one electronvolt when compared to multireference CI calculations. The improved CCSD-LRT calculations exhibited errors up to about one electronvolt but were still more accurate than the CCSD-LRT without the triple excitations. These studies indicate that higher order excitations play an important part in radical excitations.

Time dependent density function theory (TDDFT) has been shown to produce good excitation energies for several closed shell systems (for some examples, see refs 22−24). Hirata and Head-Gordon[17] have recently investigated TDDFT[25−27] as a means to treat radical transitions with double and higher excitation character. TDDFT is surprisingly successful in cases that exhibit a high percentage of double excitation character. Even more recently, Guan, Casida and Salahub,[28] Broclawik and Borowski,[29] and Spielfiedel and Handy[30] have shown that TDDFT treats excitation energies of several small open shell molecules fairly well. We, therefore, investigate TDDFT in this paper as a good method to determine radical excitations. We note that TDDFT with present-day functionals performs well for predicting the energies of valence states but performs quite poorly for Rydberg states.[17] However, we are only interested in the lowest lying excited states in this investigation, which are well below the Rydberg level.

We use TDDFT to determine the absorption spectra of the phenyl, vinyl, methyl, and hydrogen peroxy radicals. TDDFT within the Tamm−Dancoff approximation provides excited states in close agreement with full TDDFT,[31] and we include these calculations as well. We additionally perform ROCIS and XCIS calculations on all of the peroxy radicals to roughly estimate the extent and effect of double excitation character.

We further aim to probe the nature of the alkyl peroxy radical absorptions by means of molecular orbital diagrams and electron attachment/detachment density diagrams.[32] The attachment/detachment diagrams pictorially represent the hole and particle densities of an electronic transition, and, thus, aid in the characterization of the excitations. We hope to better understand the origin of the visible absorption in the phenyl peroxy radical by examining the electron attachment/detachment diagrams for all of the peroxy radicals studied here and comparing them with diagrams of different radical moieties.

Electronic Structure Methods

Kohn−Sham density functional theory (DFT) with the Becke exchange functional,[33] LYP correlation functional,[34] and the 6-31G* basis set was used to optimize the ground-state structures of all radicals studied. C_s molecular symmetry was assumed for all five peroxy radicals, and the BLYP/6-31G* structures[35] were confirmed to be minima by calculation of the Hessian matrix. TDDFT and CIS methods were used to determine the absorption spectra of the radicals. These methods were implemented with the Q-Chem program package.[36]

Several basis sets were surveyed to determine the effect on the resulting TDDFT vertical excitation energies of the phenyl peroxy radical. Using the BLYP/6-31G* optimized ground state geometry, one and two sets of heavy atom diffuse functions were added to the 6-31G* basis set to determine the extent of the effect on the excited states of the radical. The Dunning aug-cc-pVDZ and aug-cc-pVTZ basis sets were also investigated for the TDDFT calculations, and the energies are presented in Table 1. The absorptions vary by approximately a tenth of an electronvolt from no diffuse functions to the addition of one set of diffuse functions on the 6-31G* basis set. However, the excitation

(15) Maurice, D.; Head-Gordon, M. *Int. J. Quantum Chem., Symp.* **1995**, *29*, 361.
(16) Maurice, D.; Head-Gordon, M. *J. Phys. Chem.* **1996**, *100*, 6131.
(17) Hirata, S.; Head-Gordon, M. *Chem. Phys. Lett.* **1999**, *302*, 375.
(18) Comeau, D. C.; Bartlett, R. J. *Chem. Phys. Lett.* **1993**, *207*, 414.
(19) Szalay, P. G. *J. Chem. Phys.* **1996**, *105*, 2735.
(20) Szalay, P. G.; Fogarasi, G.; Nemes, L. *Chem. Phys. Lett.* **1996**, *263*, 91.
(21) Szalay, P. G.; Gauss, J. *J. Chem. Phys.* **2000**, *112*, 4027.
(22) Bauernschmitt, R.; Ahlrichs, R.; Hennrich, F. H.; Kappes, M. M. *J. Am. Chem. Soc.* **1998**, *120*, 5052.
(23) Bauernschmitt, R.; Ahlrichs, R. *Chem. Phys. Lett.* **1996**, *256*, 454.
(24) Wiberg, K. B.; Stratmann, R. E.; Frisch, M. J. *Chem. Phys. Lett.* **1998**, *297*, 60.
(25) Runge, E.; Gross, E. K. U. *Phys. Rev. Lett.* **1984**, *52*, 997.
(26) Petersilka, M.; Gossmann, U.; Gross, E. K. U. *Phys. Rev. Lett.* **1996**, *76*, 1212.
(27) Casida, M. E. In *Recent Advances in Density Functional Methods, Part I*; Chong, D. P., Ed.; World Scientific: Singapore, 1995; Chapter 5.
(28) Guan, J.; Casida, M. E.; Salahub, D. R. *THEOCHEM* **2000**, *527*, 229.
(29) Broclawik, E.; Borowski, T. *Chem. Phys. Lett.* **2001**, *339*, 433.
(30) Spielfiedel, A.; Handy, N. C. *Phys. Chem. Chem. Phys.* **1999**, *1*, 2401.
(31) Hirata, S.; Head-Gordon, M. *Chem. Phys. Lett.* **1999**, *314*, 291.
(32) Head-Gordon, M.; Grana, A. M.; Maurice, D.; White, C. A. *J. Phys. Chem.* **1995**, *99*, 14261.
(33) Becke, A. D. *Phys. Rev. A* **1988**, *38*, 3098.
(34) Lee, C.; Yang, W.; Parr, R. G. *Phys. Rev. B* **1988**, *37*, 785.
(35) See Supporting Information Tables 1−4 for BLYP/6-31G* peroxy radical structures.
(36) Kong, J.; White, C. A.; Krylov, A. I.; Sherrill, C. D.; Adamson, R. D.; Furlani, T. R.; Lee, M. S.; Lee, A. M.; Gwaltney, S. R.; Adams, T. R.; Ochsenfeld, C.; Gilbert, A. T. B.; Kedziora, G. S.; Rassolov, V. A.; Maurice, D. R.; Nair, N.; Shao, Y.; Besley, N. A.; Maslen, P. E.; Dombroski, J. P.; Dachsel, H.; Zhang, W. M.; Korambath, P. P.; Baker, J.; Byrd, E. F. C.; Van Voorhis, T.; Oumi, M.; Hirata, S.; Hsu, C. P.; Ishikawa, N.; Florian, J.; Warshel, A.; Johnson, B. G.; Gill, P. M. W.; Head-Gordon, M.; Pople, J. A. *J. Comput. Chem.* **2000**, *21*, 1532.

Table 1. Phenyl Peroxy Radical TDDFT Energies with Additional Diffuse Function Basis Sets

	$1^2A''$ ground state, energies in eV		
	$1^2A'$	$2^2A''$	$3^2A''$
6-31G*	1.1500	2.2485	2.5791
6-31+G*	1.1414	2.1133	2.4641
6-31++G*	1.1409	2.1155	2.4648
aug-cc-pVDZ	1.1341	2.1336	2.4607
aug-cc-pVTZ	1.1416	2.1401	2.4578

Table 2. Hydrogen Peroxy Radical Excitation Energies[a]

	$1^2A''$ ground state, energies in eV					
	$1^2A'$		$2^2A''$		$2^2A'$	
ROCIS	0.6359	(0.0000)	9.0237	(0.0225)	6.6972	(0.0058)
XCIS	0.4325	(0.0000)	7.1881	(0.0245)	6.1805	(0.0045)
TDDFT/TDA	1.2230	(0.0000)	6.1501[b]	(0.0354)[b]	6.1590	(0.0006)
TDDFT	1.1794	(0.0000)	5.9288[b]	(0.0559)[b]	6.1346	(0.0008)
ROHF (ref 4)			5.9644			
MP2 (ref 4)			6.0784			
MCSCF (ref 4)			5.3610			
expt (ref 1)			5.9048			

[a] Oscillator strengths given in parentheses when available. [b] TDDFT/TDA $< S^2 > = 0.8659$.

energies change by only thousandths, or at most hundredths, of an electronvolt upon addition of the second set of diffuse functions or by changing to the Dunning basis sets. Therefore, the relatively small 6-31+G* basis is satisfactory for these excited-state calculations. All CIS and TDDFT vertical excitation energies are calculated with the 6-31+G* basis set.

We examine the nature of the peroxy radical absorptions with attachment/detachment density diagrams. These densities are calculated at the BLYP/6-31+G*//BLYP/6-31G* level of theory. The visible transition densities of the phenyl peroxy radical are compared against corresponding transition densities of two phenyl species with different radical moieties, C_7H_8N and C_8H_9. These radical absorptions are calculated at the same level of theory as the peroxy radicals.

Results and Discussion

Results. The absorption spectra of the peroxy radicals calculated in this study are compared against experiment and previous calculations in Tables 2−6. The absorption of interest is the phenyl peroxy radical visible excitation, which is a transition of symmetry $1^2A'' \rightarrow 3^2A''$. All of the peroxy ground states are $1^2A''$. The $^2A''$ excited state that corresponds to the phenyl visible absorption is the $2^2A''$ state in the other peroxy radicals. This is either the second or third excited state, depending on the radical and the method. Thus, the first three excited states are shown in each table.

The hydrogen peroxy radical results for the first three excited states are shown in Table 2. The TDDFT energy agrees remarkably with experiment, whereas the XCIS and ROCIS results are too high. It should be noted that the TDDFT $2^2A''$ reference state is spin-contaminated. The S^2 operator eigenvalue is not computed for the TDDFT excited states; however, it is for the TDDFT/TDA excited states and yields 0.8659 for this state. This value is computed with the reference wavefunction and is not the true DFT S^2 value for the excited state, and so, the significance of this spin-contamination is not certain.

The methyl peroxy radical, Table 3, shows good agreement of TDDFT energy with experiment, to within ∼0.3 eV. The MCSCF calculation agrees slightly better with experiment than the TDDFT calculation; however, the MP2 and ROHF are not nearly as accurate. XCIS and ROCIS perform quite poorly, missing the absorption by several electronvolts.

Table 3. Methyl Peroxy Radical Excitation Energies[a]

	$1^2A''$ ground state, energies in eV					
	$1^2A'$		$2^2A''$		$2^2A'$	
ROCIS	0.6180	(0.0000)	7.8950	(0.0291)	6.4280	(0.0065)
XCIS	0.4080	(0.0000)	6.4109	(0.0282)	5.8939	(0.0050)
TDDFT/TDA	1.2349	(0.0000)	5.1062	(0.0446)	5.1270	(0.0013)
TDDFT	1.1971	(0.0000)	4.8727	(0.0394)	5.1048	(0.0012)
ROHF (ref 4)	5.9644					
MP2 (ref 4)	6.0784					
MCSCF (ref 4)	5.3610					
expt (ref 1)	5.1667					

[a] Oscillator strengths given in parentheses when available.

The agreement between TDDFT and experiment is not as impressive for the vinyl peroxy radicals as it is for the methyl peroxy radical. The TDDFT prediction of the *trans*-vinyl peroxy radical $1^2A'' \rightarrow 2^2A''$ absorption, excited-state 2, is low by ∼0.7 eV (see Table 4). The corresponding *cis*-vinyl absorption, Table 5, shows TDDFT to be low by ∼0.4 eV. This is better; however, it is still not as close as the previous MCSCF vertical excitation calculations predicted.[4,10] It is interesting to note that the MCSCF adiabatic excitation energy in a larger active space is not as accurate as the vertical excitation energy. Despite the quantitative error of the TDDFT results, the qualitative trend is still correct. The *trans*-vinyl excitation energy is less energetic than the UV methyl absorption and close to the visible spectrum. The *cis*-vinyl absorption is at the high energy end of the visible region, lower in energy than the *trans*-vinyl absorption. This trend is predicted by TDDFT and ROCIS as well, although ROCIS overestimates the energies by approximately 3 eV. The XCIS energies are too high by 1−2 eV and do not predict this trend.

The phenyl peroxy radical, Table 6, shows excellent agreement between TDDFT and experiment. The TDDFT absorption is less than 0.1 eV higher in energy than the experimental value. The previous MCSCF vertical excitation calculations[10] are approximately 1 eV high in energy. This is interesting, considering the success of this method for the vinyl peroxy radical absorptions. The failure of the MCSCF calculation for the phenyl peroxy radical must be related to an incomplete description of the active space required for this molecule. The XCIS and ROCIS predictions are again several electronvolts high of the experimental value.

A summary of the peroxy radical calculations performed in this study is presented in Table 7. These five radicals show a trend of decreasing excitation energy in the $1^2A'' \rightarrow 2(\text{or } 3)^2A''$ transition from the hydrogen peroxy radical, absorbing in the UV region, to the phenyl peroxy radical, absorbing in the visible region. TDDFT performed reasonably well in matching the experimental results of all of the peroxy radicals. While the method did not predict absorptions as precisely for the vinyl peroxy radicals as for the methyl and phenyl peroxy radicals, it was still qualitatively accurate. We note that the ROCIS results are also qualitatively correct in predicting the proper energetic trend, however quantitatively poor. The XCIS results do not show the correct trend in energies, although the absolute error compared to experiment is reduced slightly from ROCIS in the transitions with increased double excitation character. The TDDFT results are equally good for the excitations with both small and large double excitation character.

Characterization of the Transition. The trend in absorption energy of the $1^2A'' \rightarrow 2(\text{or } 3)^2A''$ transition is especially interesting when contrasted against the $1^2A'' \rightarrow 1^2A'$ transition of each of the peroxy radicals. On the basis of calculated excitation amplitudes, the former is essentially the promotion

Table 4. *trans*-Vinyl Peroxy Radical Excitation Energies[a]

	$1^2A''$ ground state, energies in eV					
	$1^2A'$		$2^2A''$		$2^2A'$	
ROCIS	0.6531	(0.0000)	6.7779	(0.1245)	6.5605	(0.0078)
XCIS	0.4530	(0.0000)	5.4505	(0.0773)	6.0012	(0.0054)
TDDFT/TDA	1.2364	(0.0000)	3.2085	(0.0896)		
TDDFT	1.2034	(0.0000)	2.9328	(0.0652)		
(15,11)DZd-MCSCF[b] (ref 10)			3.2444		4.9859	
(23,14)DZd-MCSCF[c] (ref 10)			2.5399		4.1402	
(15,11)DZd-MCSCF (ref 4)			3.2970			
expt (ref 4)			3.6471			

[a] Oscillator strengths given in parentheses when available. [b] (15,11) indicates 15 electrons in 11 orbitals active space MCSCF. [c] Adiabatic excitation.

Table 5. *cis*-Vinyl Peroxy Radical Excitation Energies[a]

	$1^2A''$ ground state, energies in eV					
	$1^2A'$		$2^2A''$		$2^2A'$	
ROCIS	0.5587	(0.0000)	6.3956	(0.1046)	6.4965	(0.0054)
XCIS	0.3550	(0.0000)	5.5532	(0.0493)	5.9442	(0.0043)
TDDFT/TDA	1.0696	(0.0000)	2.8385	(0.0563)		
TDDFT	1.0353	(0.0000)	2.5743	(0.0380)		
(15,11)DZd-MCSCF[b] (ref 10)			2.8837		5.1050	
(23,14)DZd-MCSCF[c] (ref 10)			2.3326		4.2437	
(15,11)DZd-MCSCF (ref 4)			2.9729			
expt (ref 4)			2.9524			

[a] Oscillator strengths given in parentheses when available. [b] (15,11) indicates 15 electrons in 11 orbitals active space MCSCF. [c] Adiabatic excitation.

Table 6. Phenyl Peroxy Radical Excitation Energies[a]

	$1^2A''$ ground state, energies in eV					
	$1^2A'$		$2^2A''$		$3^2A''$	
ROCIS	0.6168	(0.0000)	5.8685	(0.0270)	6.0200	(0.0198)
XCIS	0.4131	(0.0000)	3.0865	(0.0010)	4.4457	(0.0086)
TDDFT/TDA	1.1731	(0.0000)	2.1481	(0.0019)	2.6888	(0.1107)
TDDFT	1.1414	(0.0000)	2.1133	(0.0020)	2.4641	(0.0746)
(15,11)DZ-ROHF[b] (ref 10)	0.6535				3.5791	
(15,11)DZ-MCSCF (ref 10)	0.5194				3.4349	
(15,11)DZd-ROHF (ref 10)	0.6834				3.6839	
expt (ref 5)					2.4980	

[a] Oscillator strengths given in parentheses when available. [b] (15,11) indicates 15 electrons in 11 orbitals active space MCSCF, the level of theory stated refers to structure optimization.

Table 7. Peroxy Radical Excitation Energies

		excitation energies (eV)					
peroxy radical	state	ROCIS	XCIS	TDDFT/TDA	TDDFT	expt	% XCIS character
HO_2	$A''(2)$	9.0237	7.1881	6.1501[a]	5.9288[a]	5.9048	9.0
CH_3O_2	$A''(2)$	7.8950	6.4109	5.1062	4.8727	5.1667	8.0
trans-$C_2H_3O_2$	$A''(2)$	6.7779	5.4505	3.2085	2.9328	3.6471	17.1
cis-$C_2H_3O_2$	$A''(2)$	6.3956	5.5532	2.8385	2.5743	2.9524	24.6
$C_6H_5O_2$	$A''(3)$	6.0200	4.4457	2.6888	2.4641	2.4980	75.3

[a] TDDFT/TDA $\langle S^2 \rangle = 0.8659$.

of a β electron from the second highest doubly occupied molecular orbital (2HOMO) to the singly occupied molecular orbital (SOMO) in each radical, while the latter is the β electron HOMO to SOMO excitation, in the TDDFT picture. These two transition energies are compared in Figure 1. The trend across the peroxy radicals is quite different for the HOMO → SOMO transition than for the 2HOMO → SOMO. As discussed above, the 2HOMO → SOMO excitation decreases in energy from the hydrogen to phenyl peroxy radical. On the other hand, the HOMO → SOMO transition energy is effectively constant across the peroxy radicals, at approximately 1.1 eV.

The question is, then, why one transition is unaffected by the alkyl substituent, while the other is greatly affected. And a more fundamental question is simply what the origin of the phenyl peroxy radical visible absorption is. To begin to answer these questions, we looked at the orbital eigenvalues of the MOs involved in the transitions.[37] Figure 2 shows the orbital eigenvalues of the singly occupied MO (SOMO), highest doubly occupied MO (HOMO), and second highest doubly occupied MO (2HOMO). We note that the orbitals are unrestricted, and because the transitions of interest are in the β space, we report only the β orbital eigenvalues. If we restrict our consideration to the β space alone, the SOMO should actually be referred to as the β lowest unoccupied MO (LUMO). However, we keep the SOMO designation for clarity.

(37) See Supporting Information Table 5 for BLYP/6-31G* β orbital eigenvalues of the peroxy radicals SOMO, HOMO, and 2HOMO.

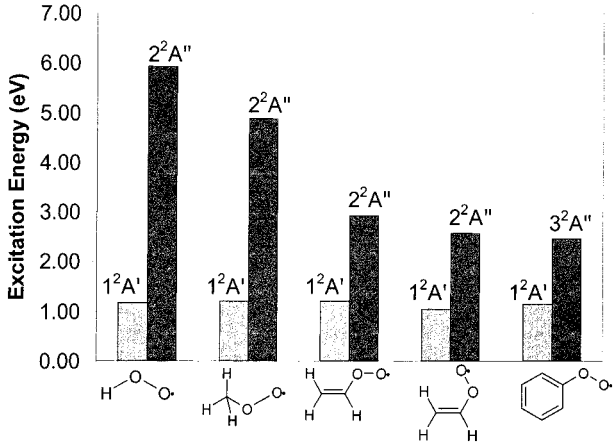

Figure 1. BLYP/6-31+G*//BLYP/6-31G* excitation energies to the $1^2A'$ and $2(\text{or } 3)^2A''$ states of the peroxy radicals.

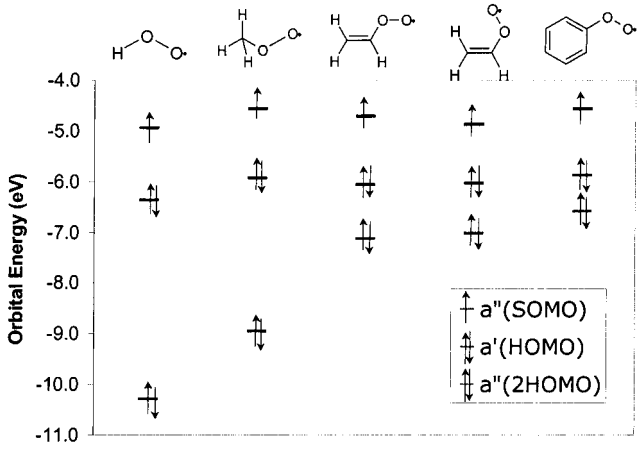

Figure 2. BLYP/6-31+G*//BLYP/6-31G* β SOMO, HOMO, and 2HOMO eigenvalues for the peroxy radicals.

The fact that the $1^2A'' \rightarrow 1^2A'$ excitation is of constant energy for all of the peroxy radicals should lead one to believe that the HOMO and SOMO energies are either fairly constant themselves across the different peroxy radicals or they shift together. Figure 2 shows that the former is true: the HOMO and SOMO eigenvalues are roughly unchanged from one peroxy radical to the next. We further see from these eigenvalues that the trend in the $1^2A'' \rightarrow 2(\text{or } 3)^2A''$ transition energy is due to the variation in the 2HOMO energy. The next question to address, then, is why the SOMO, HOMO, and 2HOMO behave so differently. The first step in trying to understand this is to simply look at the character of these orbitals.

The β 2HOMO, HOMO, and SOMO squared MO plots for each of the peroxy radicals are shown in Figure 3. It is clear from these diagrams that the 2HOMO is predominantly π in character and the SOMO is π^* in character for each of the peroxy radicals. The HOMO appears to be σ^* along the R−O bond and nonbonding on the oxygen atoms. Upon closer inspection, it is noteworthy that the HOMO is relatively unchanged with the different alkyl groups; the orbital remains located on the R−O bond and oxygen atoms. The SOMO is also very similar for all of the radicals. The peroxy group is consistently π^* on each radical with some π^* character appearing on all of the alkyl groups except for the hydrogen atom. The 2HOMO, however, does change substantially with different alkyl substituents.

Starting with the hydrogen peroxy radical, the 2HOMO is purely π on the peroxy group. The methyl peroxy radical

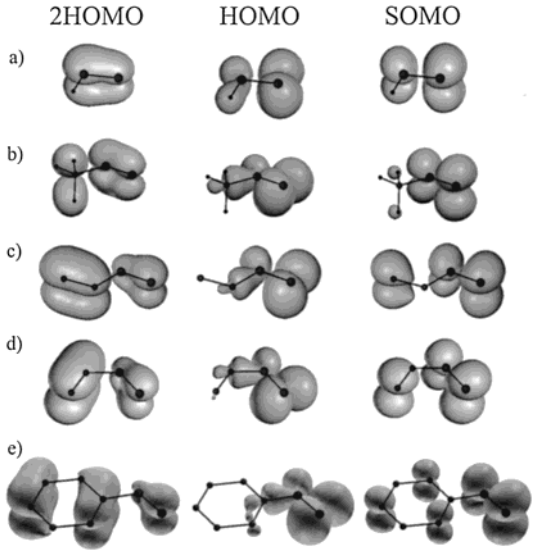

Figure 3. BLYP/6-31+G*//BLYP/6-31G* 2HOMO, HOMO, and SOMO plots of the peroxy radicals: (a) HO_2, (b) CH_3O_2, (c) *trans*-$C_2H_3O_2$, (d) *cis*-$C_2H_3O_2$, and (e) $C_6H_5O_2$.

2HOMO is still predominantly π on the peroxy group, but there is additionally some charge density on the methyl carbon. The vinyl peroxy radicals both show a significant shift of the 2HOMO π density to the vinyl group, with the peroxy group π density diminished on the connecting oxygen. The phenyl peroxy radical 2HOMO has even less π character on the connecting oxygen and increased π density on the phenyl ring. This 2HOMO shift of π character on the peroxy group of the hydrogen peroxy radical to the alkyl group of the conjugated carbon peroxy radicals is significantly different from the HOMO and SOMO of each radical, which are essentially unchanged. The change in orbital character of the 2HOMO is evidently due to mixing of the peroxy group and alkyl group orbitals across the molecule that does not occur for the HOMO and SOMO.

All of the preceding discussion on the energy trend of the $1^2A'' \rightarrow 2(\text{or } 3)^2A''$ transition versus the $1^2A'' \rightarrow 1^2A'$ transition relied on the assertion that these excitations are 2HOMO to SOMO and HOMO to SOMO, respectively. It is reasonable to question whether these transitions are simply electron density transfers from one MO to another. This may be confirmed by calculating the attachment/detachment density diagrams[32] for the transitions. We do this for the $1^2A'' \rightarrow 2(\text{or } 3)^2A''$ transition to confirm that it is essentially a 2HOMO to SOMO excitation. Attachment/detachment densities of the β electron excitation for the five peroxy radicals are shown at 90% density enclosure in Figure 4. The detachment density, placed on the left, is essentially the hole density. This is the occupied portion of the electronic ground state density that moves during the excitation. The attachment density, placed on the right, is the particle density. The particle density is associated with previously empty levels that become (fractionally) occupied upon excitation. The electron density that remains unchanged between the ground and excited states is not shown in these diagrams. The integral of these densities over all space is slightly more than 1 electron.

Attachment/detachment density analyses of the peroxy radicals show that the $1^2A'' \rightarrow 2(\text{or } 3)^2A''$ transition, as well as the $1^2A'' \rightarrow 1^2A'$ transition, is primarily excitation of the β electron, as can be seen by the largest α and β electron eigenvalues given in Table 8. Comparing the attachment/detachment densities in Figure 4 with the orbitals in Figure 3 confirms that the $1^2A'' \rightarrow 2(\text{or } 3)^2A''$ transition is the β electron 2HOMO to SOMO excitation. So, we can assert that the origin of the visible

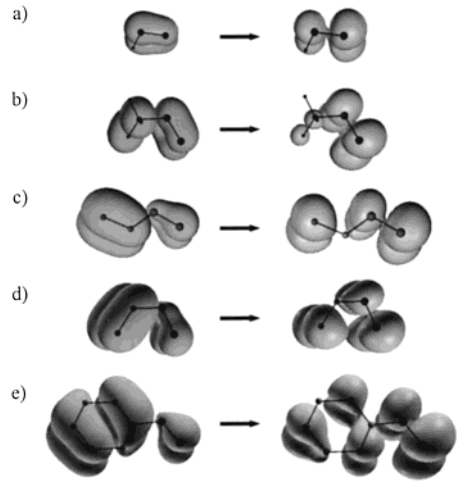

Figure 4. BLYP/6-31+G*//BLYP/6-31G* attachment/detachment densities of the peroxy radicals: (a) HO_2, (b) CH_3O_2, (c) *trans*-$C_2H_3O_2$, (d) *cis*-$C_2H_3O_2$, and (e) $C_6H_5O_2$.

Table 8. Attachment/Detachment Density Analysis of the Peroxy Radicals[a]

	$1^2A'$		$2(\text{or } 3)^2A''$	
peroxy radical	$\lambda(A)_\beta$	$\lambda(D)_\beta$	$\lambda(A)_\beta$	$\lambda(D)_\beta$
hydrogen	1.007	1.007	0.924	0.924
methyl	1.005	1.005	0.960	0.960
trans-vinyl	1.003	1.003	0.928	0.928
cis-vinyl	1.004	1.004	0.956	0.956
phenyl	1.003	1.003	0.968	0.968

[a] Largest eigenvalues, λ, are given in units of electronic charge. Eigenvalues less than 0.1 e are omitted; therefore, no α eigenvalues are shown.

absorptions in the *cis*-vinyl and phenyl peroxy radicals is rooted in the mixing of the peroxy and alkyl group orbitals to yield the alkyl peroxy radical 2HOMO. It remains to understand the origin of this mixing and why it does not occur in the HOMO and SOMO.

Qualitative Interpretation. We must confirm the assertion of orbital mixing across the alkyl and peroxy substituents to fully explain the trend in 2HOMO energies of the five peroxy radicals studied here. We do this by examining the higher occupied orbitals of the appropriate separated substituents, where the parent peroxy orbitals are those of the hydrogen peroxy radical and, likewise, the peroxy group is replaced by a hydrogen on the corresponding alkyl substituents. So, we investigate the orbitals of HO_2 along with the orbitals of CH_4, C_2H_4, and C_6H_6.[38] We have already indicated the relevant peroxy orbitals in Figure 2 as the a″(SOMO), a′(HOMO), and a″(2HOMO). From the squared MO plots in Figure 3, we determined that these orbitals are π^*, σ^* and nonbonding, and π in character, respectively. Any interaction of these peroxy orbitals with the alkyl substituent orbitals must depend on the alkyl orbitals being close in energy to the peroxy orbitals and also having appropriate overlap and symmetry.

We can first consider the very simplest approximation of the alkyl peroxy orbitals as being the unperturbed, separated, substituent orbitals. In this picture, the alkyl peroxy radical SOMO, HOMO, and 2HOMO are unmixed orbitals on either the peroxy or alkyl substituent. This zeroth order picture works fairly well for the a″(SOMO) and a′(HOMO) of each alkyl peroxy radical as simply being the peroxy a″(SOMO) and a′-(HOMO), see Figures 5−7. The orbital energies are close, within 0.5 eV, and the orbital character is similar for each, as seen in Figure 3. Note that the substituent fragments do not have the same molecular symmetry; however, each molecule does have a common plane of symmetry. So, for simplicity, we refer to the orbitals in terms of their planar symmetry.

The zeroth order picture also works reasonably well to describe the alkyl peroxy radical a″(2HOMO) level. It is easiest to see with the ethene and benzene substituents that the a″-(2HOMO) energy of the alkyl peroxy radical is approximately

(38) See Supporting Information Tables 6−8 for BLYP/6-31G* β orbital eigenvalues of peroxy with phenyl, vinyl, and methyl substituents.

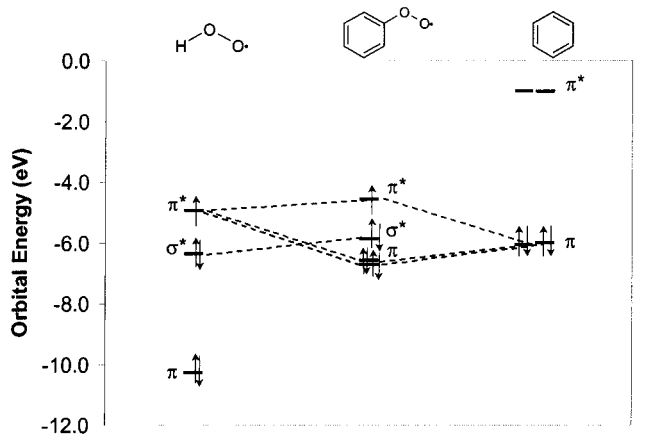

Figure 5. Qualitative picture of phenyl and peroxy substituent orbital mixing.

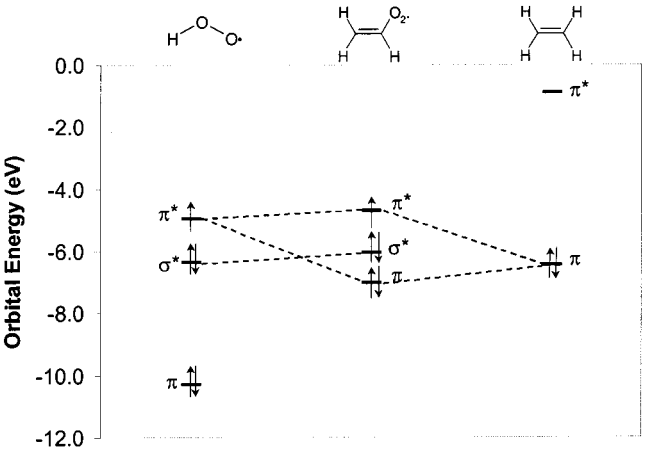

Figure 6. Qualitative picture of vinyl and peroxy substituent orbital mixing.

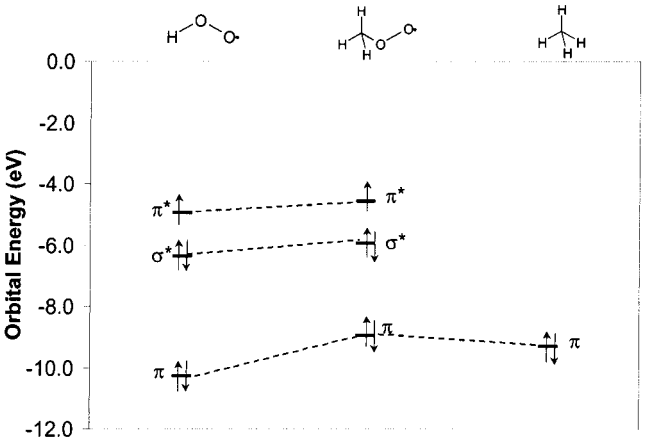

Figure 7. Qualitative picture of methyl and peroxy substituent orbital mixing.

0.5 eV lower than that of the alkyl substituent π-type HOMO. This is also true for methane when we consider that the π-type orbital should be able to mix with the peroxy π-type orbitals once the C_{3v} symmetry is broken; however, the methyl peroxy orbital is shifted 0.5 eV higher in energy, rather than lower, than the methane orbital.

We can then get a better picture of the alkyl peroxy radical a″(2HOMO) with the next simplest approximation, and that is to allow the π-type orbitals on the peroxy and alkyl substituents to interact. This resulting orbital will be a mixture of the peroxy a″(SOMO) and a″(2HOMO), and the alkyl substituent LUMO and HOMO. The orbitals which will interact most strongly will be those orbitals closest in energy. For benzene and ethene, the peroxy a″(SOMO) and alkyl HOMO are more than twice as close in energy as the other π-type orbitals. So, in the simplest orbital mixing picture, the alkyl peroxy radical a″(2HOMO) will result from the peroxy a″(SOMO) and alkyl HOMO pushing each other apart, thus yielding a 2HOMO that is lower in energy than the alkyl HOMO. This orbital predominantly takes the alkyl HOMO character; however, it also receives some character from the peroxy a″(SOMO). Simple orbital energy diagrams to illustrate this mixing picture are shown in Figures 5 and 6 for benzene and ethene, respectively. So, this explains the orbital diagrams in which the peroxy group π density shifts away from the connecting oxygen, as discussed earlier and shown in Figure 3.

The interaction of the peroxy a″(SOMO) and alkyl (benzene and ethene) HOMO also explains the alkyl peroxy radical a″-(SOMO). This orbital should be the perturbed orbital that has been pushed higher in energy, where the alkyl peroxy radical a″(2HOMO) was the perturbed orbital that was pushed lower in energy. This alkyl peroxy radical a″(SOMO) will predominantly resemble the peroxy a″(SOMO), with some character coming from further mixing with the alkyl LUMO, which is π^* in nature. This is exactly what we see for the vinyl and phenyl peroxy radical SOMOs and what was previously discussed in regards to Figure 3.

The methyl peroxy radical orbitals may be similarly explained; however, the prominent orbitals involved in mixing are not the same as for the vinyl and phenyl peroxy radicals. Figure 7 shows the orbital energy diagrams of the methyl and peroxy substituents. The orbitals closest in energy are the peroxy a″(2HOMO) and methane π-type HOMO; the peroxy a″-(SOMO) is not one of the main orbitals in the mixing picture. So, the methyl peroxy radical a″(2HOMO) results from the peroxy a″(2HOMO) and methane π-type HOMO pushing each other apart: the methyl peroxy radical a″(2HOMO) is the orbital that has been pushed higher in energy. This orbital retains the character of both substituent orbitals and should, therefore, have π density on both the methyl and peroxy parts of the molecule. Once again, this is what we have seen in Figure 3. Further interaction of this orbital with the peroxy a″(SOMO) yields a methyl peroxy radical a″(SOMO) that is shifted slightly higher in energy than the peroxy a″(SOMO), yet retains most of its character.

The simple orbital mixing picture does a satisfactory job of qualitatively explaining why it is that the alkyl peroxy radical SOMO and HOMO are relatively unaffected by changing alkyl substituents, whereas the 2HOMO is greatly affected. We can therefore confirm the previous assertion that orbital mixing is responsible for the origin of the visible absorptions in the *cis*-vinyl and phenyl peroxy radicals. Because it is necessary for the orbital energies of the peroxy and alkyl substituents to be close in order to significantly interact, we have established the necessity of particular alkyl substituents, namely the *cis*-vinyl and phenyl substituents, to yield a visible absorption. Equipped with this knowledge, we can investigate and predict the role of the peroxy substituent in producing a visible absorption. We do so by comparing the phenyl peroxy radical to two other isoelectronic phenyl radicals, C_7H_8N and C_8H_9. In these molecules, the peroxy group has been replaced by CH_2NH and CH_2CH_2, respectively.

Table 9. Survey of Phenyl with Radical Moiety Absorptions

radical	state	excitation energy[a] (eV)	oscillator strength[a]
$C_6H_5O_2$	$3^2A''$	2.4641	0.0746
C_7H_8N	3^2A	2.4586	0.0064
C_8H_9	3^2A	3.4367	0.0024

[a] Reported at the BLYP/6-31+G*//BLYP/6-31G* level.

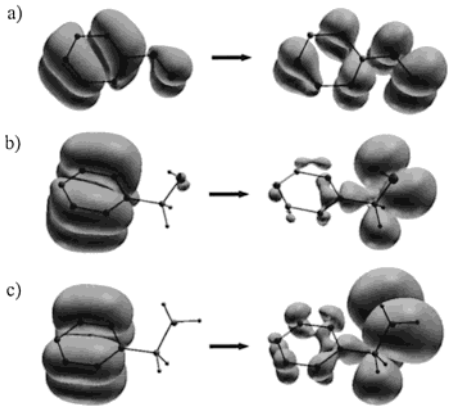

Figure 8. BLYP/6-31+G*//BLYP/6-31G* attachment/detachment densities of the phenyl based radicals with different radical moieties: (a) $C_6H_5O_2$, (b) C_7H_8N, and (c) C_8H_9.

Related Systems. Table 9 compares the second highest doubly occupied to singly occupied electronic absorption energies and oscillator strengths of the three phenyl-based radicals. The peroxy and nitrogen based radical absorptions are essentially the same energy in the visible region while the alkyl radical absorption is approximately 1 eV higher in energy, in the UV region. An important distinction that sets the phenyl peroxy radical apart from the other two radicals is that its oscillator strength for this transition is over 1 order of magnitude larger than that of the others.

Attachment/detachment densities of the second highest doubly occupied to singly occupied β electron transition for the phenyl-based radicals are shown in Figure 8. The C_7H_8N and C_8H_9 radicals have no molecular symmetry, so the corresponding transition is $1^2A \rightarrow 3^2A$ for both species. The transition densities of these two radicals are notably different from the peroxy radical transition. All three radicals exhibit π detachment character on the phenyl group; however, the peroxy radical group also has π detachment character, whereas the other two radical groups have essentially no detachment density. The attachment densities are also very different. The phenyl peroxy radical has π^* attachment character on both the phenyl and peroxy radical portions of the molecule. The other two radicals have very little π^* attachment density on the phenyl ring that has more nodes than on the phenyl peroxy radical. Furthermore, the attachment densities of the radical portions are much larger and are σ^* and nonbonding in character. This density transfer across the molecule in the C_7H_8N and C_8H_9 radicals explains the lower oscillator strength compared to the phenyl peroxy radical.

In fact, we could have predicted this behavior of the peroxy radical group versus the two other radical groups by an orbital

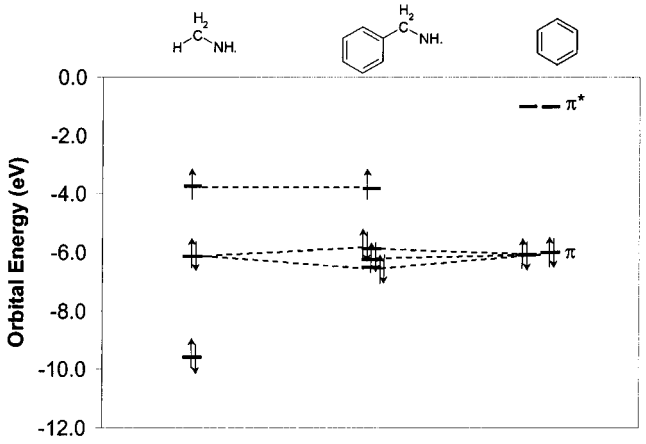

Figure 9. Qualitative picture of phenyl and CH_3NH substituent orbital mixing.

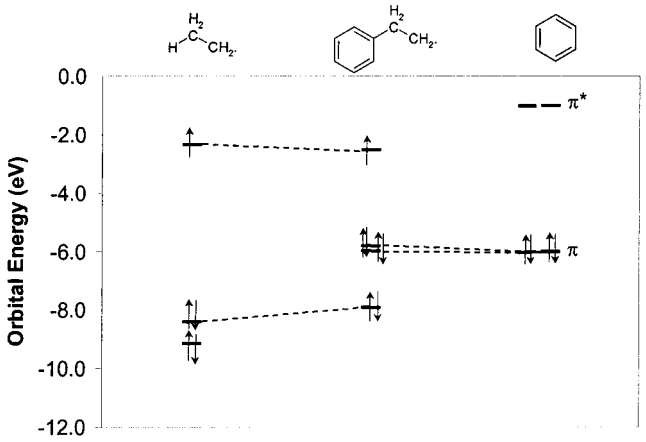

Figure 10. Qualitative picture of phenyl and CH_3CH_2 substituent orbital mixing.

energy consideration, as we did with the alkyl peroxy radicals. We begin once again with a no orbital mixing picture of benzene with CH_2NH and CH_2CH_2,[39] in this case, to explain the SOMO, HOMO, and 2HOMO of the two new substituted phenyl radicals. Simply on the basis of the orbital energy levels, we may conclude that the phenyl radical a(SOMO) is the radical substituent (CH_2NH and CH_2CH_2) a(SOMO) for both C_7H_8N and C_8H_9, as shown in Figures 9 and 10, respectively. The benzene substituent LUMO is higher in energy and is, therefore, a higher unoccupied orbital. The two next lower energy orbitals come from the benzene substituent (the doubly degenerate π-type orbitals) for C_8H_9, and both the benzene and CH_2NH substituents for C_7H_8N. These must become the a(HOMO) and a(2HOMO) of the substituted phenyl radicals. When we compare the benzene degenerate HOMOs to the a(HOMO) and a(2HOMO) of the substituted phenyl radicals, we see that the a(2HOMO) matches this energy for both phenyl radicals. The a(HOMO) is slightly higher in energy and clearly results from a breaking of the D_{6h} symmetry of benzene when the radical substituent replaces a hydrogen. In the case of C_7H_8N, there may also be some orbital mixing between one of the benzene degenerate HOMOs and the CH_2NH a(HOMO). The zeroth order picture of no orbital mixing should be sufficient for these two substituted phenyl radicals, because the two orbitals involved in the transition of interest match energies so well with unperturbed substituent orbitals.

(39) See Supporting Information Tables 9−10 for BLYP/6-31G* β orbital eigenvalues of phenyl with CH_3NH and CH_3CH_2 substituents.

The important orbitals to consider in predicting the substituted phenyl radicals versus the phenyl peroxy radical are the SOMO and 2HOMO. In both C_7H_8N and C_8H_9, the SOMO is the radical substituent SOMO, and the 2HOMO is the unperturbed benzene HOMO. The $1^2A \rightarrow 3^2A$ transition, 2HOMO to SOMO, should therefore reflect that the electron density is shifting from the phenyl group to the radical group. This is exactly what we have seen in the attachment/detachment diagrams in Figure 8. In contrast, the phenyl peroxy radical SOMO and 2HOMO resulted from orbital mixing across the two substituents, as is observed in the fact that these orbitals are not localized on one side or the other of this molecule. This makes absolutely clear the role of the peroxy radical group in the origin of the visible absorption. In the case of a phenyl based radical, the radical group must have orbitals that are close in energy to the benzene HOMO and be of appropriate symmetry to mix with this π-type orbital.

Conclusions

Time dependent density functional theory successfully predicts the experimentally observed visible absorption of the phenyl peroxy radical, in contrast to previous calculations. TDDFT is a suitable theory for this system, as evidenced by the absorptions of the methyl and vinyl peroxy radicals. The success seen here may be attributed to the fact that the phenyl peroxy visible absorption is an excitation to a low-lying valence state, where TDDFT is generally reliable. Further, this transition exhibits a high percentage of double excitation character as suggested by the XCIS calculations, again something that TDDFT appears to be able to describe well.

MO plots of the singly occupied molecular orbital, highest doubly occupied molecular orbital, and second highest doubly occupied molecular orbital provide insight into the origin of the visible absorption in the phenyl peroxy radical. The SOMO and HOMO of each peroxy radical are similar in both energy and character, regardless of the alkyl substituent. The SOMO and HOMO are primarily peroxy group orbitals that are σ* and nonbonding, and π* in character, respectively. These orbitals do not receive much, if any, character from the alkyl portion of the molecule, and are, therefore, relatively unaffected by changing the alkyl substituent.

The 2HOMO, however, shifts in energy and character with changing alkyl substituent. The orbital character goes from π character lying predominantly on the peroxy group to predominantly on the alkyl group, going from hydrogen to phenyl substituents. The π character diminishes in intensity on the connecting oxygen for the vinyl and phenyl peroxy radicals. We have shown that this is a result of the 2HOMO coming from a mixing of the peroxy and alkyl substituent orbitals and, so, is affected by the shifting alkyl π-type orbitals.

Attachment/detachment density diagrams of the $1^2A'' \rightarrow 2(\text{or } 3)^2A''$ electronic transition confirm that this is the β 2HOMO to SOMO excitation. These diagrams depict the electron density that moves during the excitation and confirm that only these two orbitals are involved in the transition, in the TDDFT picture. It is, therefore, the 2HOMO of the *cis*-vinyl and phenyl peroxy radical, that resulted from mixing of the alkyl and peroxy group π-type orbitals, that is responsible for the origin of the visible absorption.

The C_7H_8N and C_8H_9 radicals provide some insight concerning the role of the peroxy radical moiety in the phenyl peroxy radical visible absorption. Consideration of the substituent orbital energies and symmetries indicates the necessity of similarities between the radical and alkyl groups. While the C_8H_9 radical

absorbs in the UV, the C_7H_8N radical exhibits a TDDFT absorption at the same energy as the phenyl peroxy radical. This is simply a matter of the separated substituent orbital energies, because there is no mixing across the molecule. Because there is no orbital mixing, the transition is merely a transfer of electron density from the phenyl ring to the radical substituent. The electron transfer nature of these two radicals yields low oscillator strengths and, thus, indicates that the phenyl peroxy radical visible absorption is related specifically to the peroxy radical group, because its orbitals were able to mix with the benzene orbitals.

The value of TDDFT for quantitative calculations of valence excited states has been emphasized many times in recent years. One aspect that has not been given equal emphasis is the ease with which TDDFT calculations can be understood in simple orbital terms, because in terms of Kohn−Sham orbitals, the transitions are just single excitations. Without this simplicity, we could not so easily have extracted our qualitative picture of excitations in alkyl peroxy radicals.

Acknowledgment. This research was supported by the Director, Office of Energy Research, Office of Basic Energy Sciences, Chemical Sciences Division of the US Department of Energy, under Contract DE-AC03-76SF00098. We additionally acknowledge grants of supercomputer time from NERSC and a SUR grant from IBM for computing equipment.

Supporting Information Available: Comparisons of calculational methods and details of radical geometries (PDF). This material is available free of charge via the Internet at http://pubs.acs.org.

JA011368E